

# Probing the Hexosamine Biosynthetic Pathway in Human Tumor Cells by Multitargeted Tandem Mass Spectrometry

Anas M. Abdel Rahman,<sup>†</sup> Michael Ryczko,<sup>†,‡</sup> Judy Pawling,<sup>†</sup> and James W. Dennis<sup>\*,†,‡,§</sup>

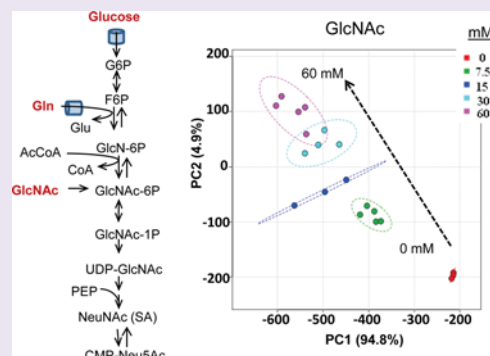
<sup>†</sup>Samuel Lunenfeld Research Institute, Mount Sinai Hospital, 600 University Ave., R988 Toronto, Ontario, Canada, M5G 1X5

<sup>‡</sup>Department of Molecular Genetics and <sup>§</sup>Department of Laboratory Medicine and Pathology, University of Toronto, Toronto, Ontario, Canada M5S 1A1

## Supporting Information

**ABSTRACT:** Cancer progression is accompanied by increases in glucose and glutamine metabolism, providing the carbon and nitrogen required in downstream anabolic pathways. Fructose-6P, glutamine, and acetyl-CoA are central metabolites and substrates of the hexosamine biosynthesis pathway (HBP) to UDP-*N*-acetylglucosamine (UDP-GlcNAc), an essential high-energy donor for protein glycosylation. Golgi and cytosolic glycosylation pathways are sensitive to UDP-GlcNAc levels, which in turn regulates metabolic homeostasis in a poorly understood manner. To study the hexosamine biosynthesis pathway in cancer cells, we developed a targeted approach for cellular metabolomics profiling by liquid chromatography–tandem mass spectrometry. Human cervical (HeLa) and prostate cancer (PC-3) cell lines were cultured in medium with increasing concentrations of glucose, glutamine, or GlcNAc to perturb the metabolic network. Principal component analysis

indicated trends that were further analyzed as individual metabolites and pathways. HeLa cell metabolism was predominantly glycolytic, while PC-3 cells showed a greater dependency on extracellular glutamine. In both cell lines, UDP-GlcNAc levels declined with glucose but not glutamine starvation, whereas glutamine abundance increased UDP-GlcNAc levels 2–3-fold. GlcNAc supplementation increased UDP-GlcNAc 4–8-fold in both HeLa and PC-3 cells. GlcNAc supplementation in HeLa cells induced nonmonotonic changes in NADH/NAD<sup>+</sup>, NADPH/NADP<sup>+</sup>, reactive oxygen species, and reduced/oxidized glutathione. In PC-3 cells, GlcNAc supplementation also increased glucose and glutamine uptake and catabolism. Our results suggest that stimulation of the HBP in cancer cells regulates metabolism and redox potential, which might be exploited to target cancer cells.



Cancer cells display altered patterns of metabolism driven by mutations in oncogenes and tumor suppressor genes. Commonly activated signaling pathways such as RAS, AKT-c-MYC, and hypoxia inducing factor (HIF1 $\alpha$ ) increase the expression of nutrient transporters and specific enzymes in anabolic pathways.<sup>1,2</sup> These changes in metabolism are often described as the Warburg effect, which diverts intermediates away from oxidation respiration in the mitochondria and into the biosynthesis of proteins, lipids, nucleic acids, and glycoconjugates.<sup>3</sup> For example, the embryonic isoform of pyruvate kinase (PKM2) has reduced enzyme activity, which results in a buildup of glycolytic intermediates that enhances anabolic metabolism.<sup>4,5</sup> The tumor suppressor p53 functions as a transcription factor, regulating genes that promote cell-cycle arrest, apoptosis, senescence but also metabolism, notably mitochondrial glutaminase (GLS2) and fructose 2,6 biphosphatase (TIGAR), which oppose the Warburg effect. Recent studies on functional domains suggest that only p53-dependent effects on metabolism are required for suppression of early onset spontaneous tumorigenesis, supporting the hypothesis that rewiring of metabolism is a driver of cancer progression.<sup>6</sup> Increased glutamine catabolism in the tricarbox-

ylic acid (TCA) cycle is anaplerotic, allowing glycolytic intermediates to be diverted into the pentose phosphate pathway (PPP), antioxidants, and other pathways.<sup>7</sup> However, metabolism varies between cancers depending on clinical type and history, including their dependency on glucose (Glc), glutamine (Gln), serine, glycine, and other nutrients.<sup>8</sup> Glc deprivation also contributes to the selection of tumor cells with K-Ras mutations, which up-regulates the GLUT1 glucose transporter.<sup>9</sup> In a tumor model driven by inducible K-Ras, metabolic profiling revealed increases in glycolysis and hexosamine biosynthesis pathway (HBP), which supplies uridine diphosphate *N*-acetylglucosamine (UDP-GlcNAc) to biosynthesis of glycoproteins.<sup>10</sup>

Cancer cell proliferation is supported by growth factor receptor signaling and nutrient transporters, which are translated in the secretory pathway and translocated to the cell surface. UDP-GlcNAc is required in the synthesis of oligosaccharide-pp-dolichol, the donor for *N*-glycosylation of

Received: December 17, 2012

Accepted: July 11, 2013

Published: July 11, 2013

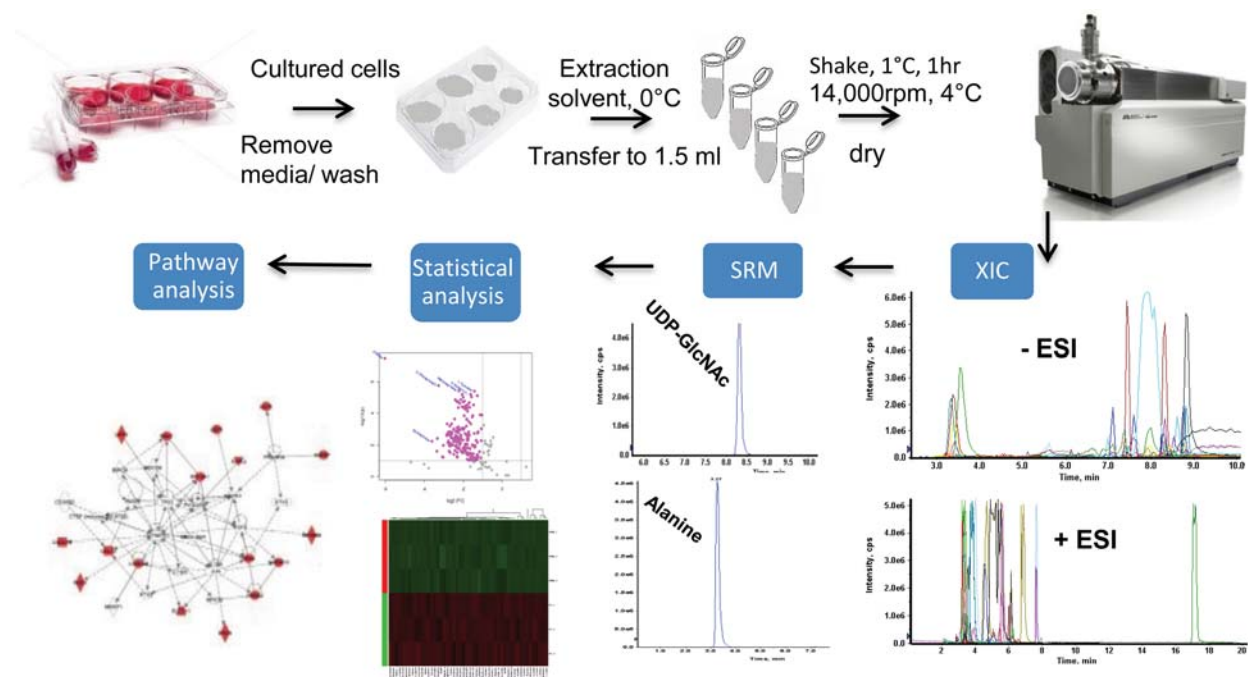


**Figure 1.** Schematic of the workflow. Metabolite extraction from cells, sample handling, and data acquisition by LC–MS/MS is followed by statistical and pathway analysis. Extracted ion chromatograms (XICs) in positive (+ESI) and negative (–ESI) mode are representative for total metabolites as well as selected reaction monitoring (SRM) chromatograms for UDP-GlcNAc and alanine.

newly synthesized proteins in the endoplasmic reticulum (ER). The oligosaccharide (or glycan) is cotranslationally substituted onto asparagines (Asn) at NXS/T sites, and the *N*-glycans play an important role in protein folding and proteostasis.<sup>11</sup> UDP-GlcNAc is also required in the Golgi *N*-glycan remodeling pathway and in the cytosol for O-GlcNAcylation of proteins.<sup>12,13</sup> Both Golgi remodeling and O-GlcNAcylation are sensitive to UDP-GlcNAc levels.<sup>12,14,15</sup> UDP-GlcNAc levels have been shown to regulate branching of *N*-glycans on cell surface receptors (EGF, PDGF, and TGF- $\beta$  receptors) and solute transporters (Glut2, Glut4).<sup>14,16</sup> The Golgi branching pathway generates *N*-glycan modifications with higher affinity for galectins, an interaction that slows glycoprotein dynamics in the lipid bilayer and loss to endocytosis, thereby increasing cell surface residency and activity.<sup>14,17,18</sup> Disrupting galectins in carcinoma cells resulted in the redistribution of more than 100 glycoproteins into lipid rafts and endosomes.<sup>17</sup> This included transporters for glucose (Slc2a1), amino acids (Slc7a5), pyruvate (Slc16a1), glutamine (Slc3a2), and iron (Slc11a2).

In the *de novo* HBP, glutamine:fructose-6P aminotransferase (GFPT) catalyzes the first committed but reversible step, conversion of fructose-6P and glutamine to glucosamine-6P and glutamate.<sup>19</sup> The next reaction is irreversible in mammalian cells and is catalyzed by glucosamine-6 phosphate *N*-acetyltransferase (*GPNAT1/GNA1*), which transfers an acetyl group from acetyl-CoA to the primary amine of glucosamine-6-phosphate (GlcN6P), producing *N*-acetylglucosamine-6-phosphate (GlcNAc-6P) and coenzyme A (CoA).<sup>20</sup> The next enzyme, phosphoacetylglucosamine mutase (PGM3), converts GlcNAc-6P to GlcNAc-1P, and finally UDP-*N*-acetylglucosamine pyrophosphorylase (UAP1) catalyzes the production of UDP-GlcNAc through the use of uridine triphosphate and GlcNAc-1P. Interestingly, *GNA1*-deficient mouse embryo fibroblasts salvage GlcNAc from serum and recycled glycoconjugates, suggesting that under normal conditions autophagy

and recycling is a significant contributor to cellular UDP-GlcNAc pool. Moreover, mammalian cells lack both a GlcNAc transporter and GlcNAc-6P *N*-deacetylase activity.<sup>21,22</sup> Therefore, GlcNAc salvaged by autophagy or extracellular uptake by fluid phase endocytosis is converted to GlcNAc-6P and contributes exclusively to UDP-GlcNAc.<sup>23</sup> These observations suggest the *de novo* and salvage pathways may differentially participate in the production of UDP-GlcNAc and exert specific adaptive effects at the cell surface over different UDP-GlcNAc concentrations.

In a recent study, GlcNAc supplementation to Glc-depleted B lymphoma cells preserved surface interleukin-3 receptor (IL3R), thereby allowing IL-3 dependent growth signaling, glutamine uptake, and rescue of cell growth (i.e., cell volume). This required GlcNAc salvage into UDP-GlcNAc and *N*-glycan branching on IL-3R and presumably other surface glycoproteins. These effects were shown to be dependent on increased glutamine uptake, and flux into the TCA cycle, as well as lipid and protein synthesis.

Metabolomics is a rapidly emerging field with the potential to comprehensively measure metabolites in cells, tissues, and fluids using techniques such as nuclear magnetic resonance (NMR) and mass spectrometry (MS). Approaches include chemometric (untargeted), which tracks all features and compares samples; subsequently, those of interest are identified. Alternately, a target list of compounds is detected and quantified on the basis of pre-established NMR or MS profiles of known standards. Herein, we explore the effects of different nutrient conditions on HeLa and PC-3 cells metabolic profiles using tandem mass spectrometry in a targeted approach. The titration of external nutrients revealed consistent changes in HBP metabolites, thereby illustrating the robustness of the method. In addition, the data revealed novel and different effects of HBP on HeLa and PC-3 cells cancer cell

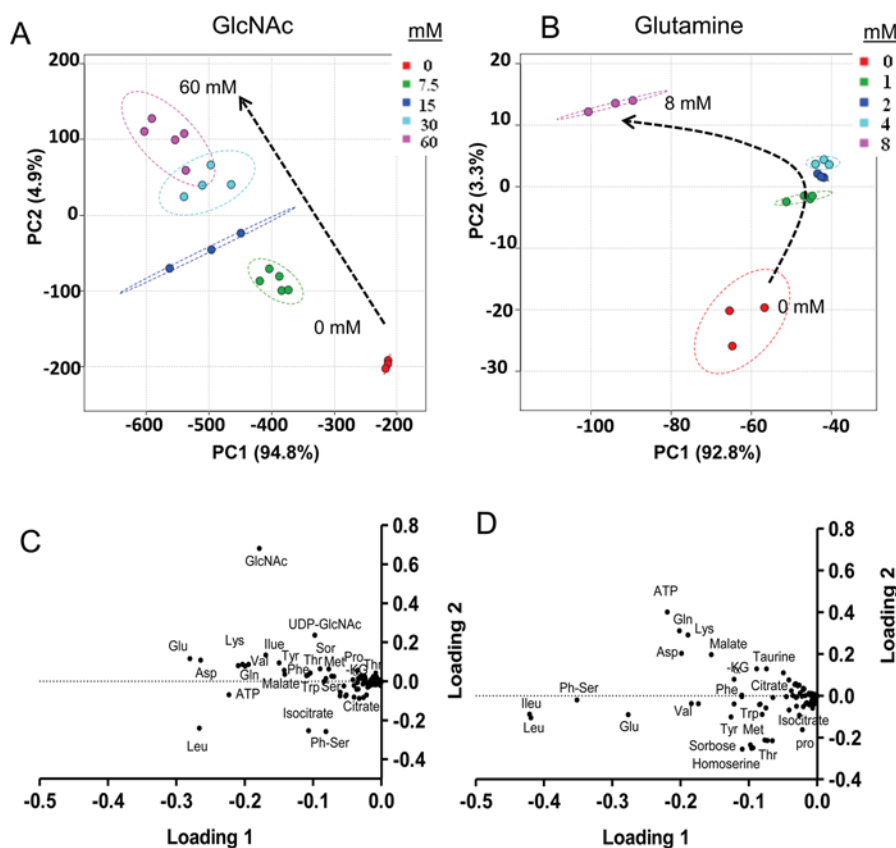


**Figure 2.** Principal component analysis (PCA). Changes in HeLa cell metabolites as a function of (A, C) GlcNAc and (B, D) glutamine titrations. The dashed arrow indicates a directional trend. Each point in panels A and B is a biological replicate, independent cultures of cells done at the same time, and the contribution of individual metabolites in each point at the PCA is displayed as a loading plot in panels C and D.

metabolism, which suggest new strategies for controlling cancer growth.

## RESULTS AND DISCUSSION

**Experimental Design and Method Development.** This study was initially designed to determine the capability, sensitivity, and reproducibility of liquid chromatography tandem mass spectrometry (LC–MS/MS) in multiple-reaction monitoring (MRM) mode for cellular metabolomic profiling. Total soluble metabolites were extracted from HeLa and PC-3 cells after culturing in medium with varying concentrations of either of GlcNAc, Gln, or Glc (Figure 1). We measured 270 metabolites in either positive or negative mode runs, and most were validated with standards as indicated in Supplementary Table S1. Data for 3–5 technical replicates were averaged, and each metabolite was evaluated for consistency and experimental trends by unsupervised principal component analysis (PCA), followed by the analysis of individual metabolites using an ANOVA test.<sup>24,25</sup> The custom library of targeted metabolites was assembled with human metabolome (HMDB) and METLIN database accession numbers.<sup>26,27</sup> The triple-quadrupole mass spectrometry parameters were generated for most of the metabolites based upon standards and empirical data in our system, which matched published data.<sup>28</sup> Compounds are identified in 3 dimensions based on LC retention times (RT), precursor ion (Q1) and product ion (Q3), under defined LC–MS/MS conditions of collision energy (CE), and declustering potential (DP) (Supplementary Table S1). The area under the peak is used to quantify each targeted compound. Calibration curves for standards were developed in mixtures using 10 times

serial dilution, to cover a wide dynamic range, and revealed accurate measures over five log decades for each metabolite. The lower limit of quantification for most metabolites was  $\sim 2$  nM, and the Pearson correlation coefficient ( $R$ ) for the best seven consecutive points was above 0.99 for the calibration curves. Inter- and intraday variability for metabolites in cell extracts was  $\leq 15\%$  in both positive and negative mode LC–MS/MS. A full validation and stability study of cultured cells, tissues, and serum is being conducted, and most of the metabolites' stability was 80–100% at the sample preparation, storage, and analysis experimental conditions.

The LC–MS/MS system does not resolve hexose and hexosamine isomers such as glucose/galactose and GlcNAc/GalNAc and their phosphorylated and sugar-nucleotide isomer forms. UDP-GlcNAc/UDP-GalNAc isomerase is widely present in mammalian cells and may maintain homeostatic balance of these nucleotide sugars. However, undetected change in the proportion of UDP-GlcNAc and UDP-GalNAc may have biological consequence in our experiments. For the purpose of discussing trends in these isomer pools, we refer to the Glc forms in the text below.<sup>28</sup>

**Hexosamine Biosynthetic Pathway (HBP).** HeLa cell growth is dependent on the catabolism of both Gln and Glc.<sup>29,30</sup> Cells were cultured for 24 h in custom DMEM medium with varying Glc, Gln, and GlcNAc concentrations. The time was chosen as sufficient to reach steady state for changes in metabolites, while minimizing the chances of selection or long-term adaptation to the new growth conditions. The modifications were made to the reference medium, DMEM containing 25 mM Glc, 2 mM Gln, and 0 mM

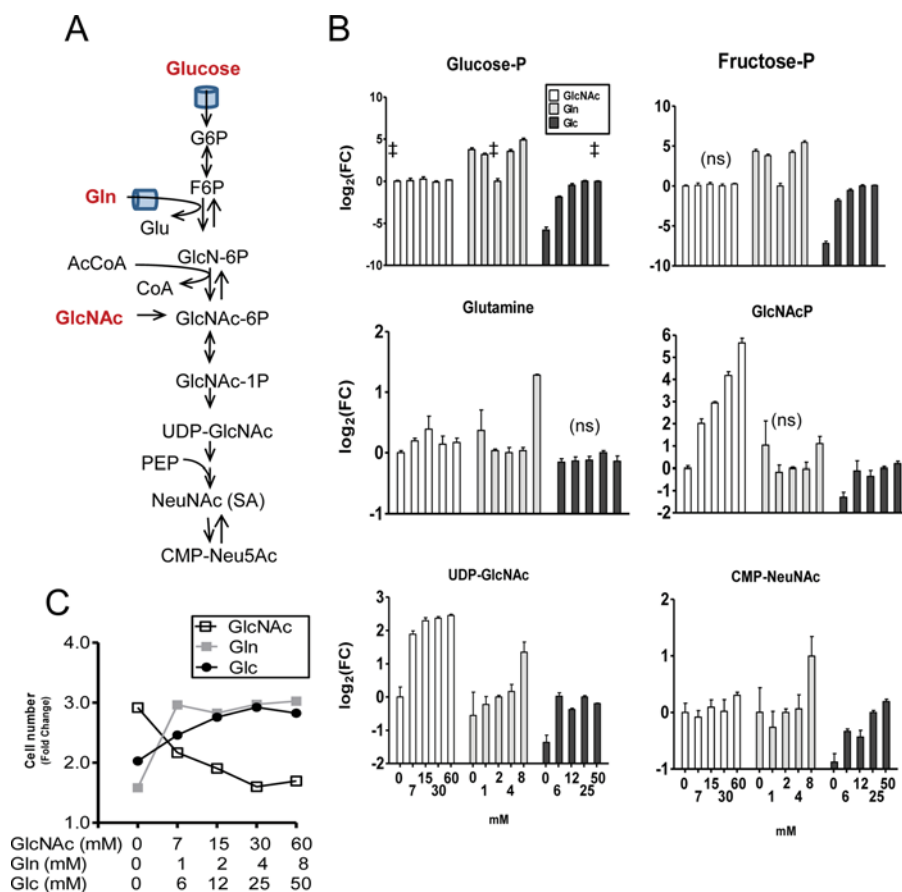


**Figure 3.** HBP in HeLa cells. (A) Pathway diagram. (B) Changes in six metabolites at five concentrations of GlcNAc, Gln, and Glc as indicated. Significant changes were evaluated by one-way ANOVA,  $P < 0.05$ , or otherwise marked as “ns” to indicate not significant. The reference culture conditions are marked by ‡, samples 1, 3, and 4 in the GlcNAc, Gln, and Glc titrations, respectively. Each series is normalized to reference culture conditions, and the y-axis is plotted at  $\log_2$ (fold change). (C) Cell number after culturing in the various conditions, as fold change over 24 h.

GlcNAc. The reference culture conditions exceed physiological concentrations of Glc and are approximately physiological for Gln. Titration of extracellular GlcNAc is expected to alter HBP metabolites in a progressive manner<sup>14,31</sup> and thereby support method validation. GlcNAc is converted exclusively into UDP-GlcNAc and not catabolized,<sup>23</sup> whereas around ~5% of Glc and Gln is required to support UDP-GlcNAc biosynthesis. Cell metabolites were extracted and analyzed by LC–MS/MS as described in Methods, and directional changes in metabolite levels as a function of supplement titration were assessed by PCA. Each principal component (PC1, PC2, ...) is a set of data parameters that change in a coordinated manner as a result of the experimental treatment. Successive PC groups decrease in statistical confidence,<sup>32</sup> where a plot of PC1 and PC2 generally captures the major trends. As shown for GlcNAc and Gln titrations, technical replicates are clustered (ellipse) and in most cases separated, indicating tolerable experimental variation. The clustered groups are ordered in a linear manner with GlcNAc supplementation and a curvilinear pattern with increasing glutamine, an interpretable trend that is reproduced with many of the individual metabolites (Figure 2A,B). Metabolites contributing to PC1 and PC2 were ranked by significance and examined individually for directional change with growth conditions (Figure 2C,D). For the GlcNAc titration, PC1 and PC2 scores are 95% and 5%, respectively, with HBP metabolites as a major contribution, although additional metabolites are included as described below.

GlcNAc salvage has the expected point of entry into the pathway, with conversion to GlcNAc-6P followed by isomerization to GlcNAc-1P, which are measured together by the LC–MS/MS method (Figure 3A). GlcNAc-P increased progressively, reaching ~50-fold at the highest levels of GlcNAc supplementation (Figure 3B). In contrast, UDP-GlcNAc increased in a hyperbolic manner with a GlcNAc  $D_{50}$  of ~5 mM and maximum of ~5.5-fold. This suggests maximum cellular UDP-GlcNAc concentrations may be limited by the activities PGM3 and UAP1 or by negative feedback on these enzymes. UDP-GlcNAc 2-epimerase/*N*-acetylmannosamine kinase generates ManNAc-6P and subsequent reactions requiring phosphoenolpyruvate (PEP) and CTP to produce CMP-Neu5Ac.<sup>33</sup> GlcNAc supplementation showed only a slight increase in CMP-Neu5Ac, but depletion of Glc depressed CMP-Neu5Ac levels more than UDP-GlcNAc. It is possible that the requirement for an additional glycolytic intermediate phosphoenolpyruvate (PEP) further suppresses CMP-Neu5Ac levels in Glc depleted conditions (Figure 3B). Glc-P and fructose-P (FruP) are upstream of GlcNAc-6P in the HBP, and levels did not change, consistent with previous observations that GlcNAc-6P is not catabolized in cultured mammalian cells and thus does not contribute directly to glycolysis.<sup>23</sup> Moreover, GlcNAc supplementation under the conditions of our reference medium (25 mM Glc) did not alter the steady-state levels of these upstream glycolytic intermediates in HeLa cells. In

contrast, GlcNAc supplementation to PC-3 cells did positively regulate glycolytic intermediates as described below.

Consistent with the substrate requirements of the *de novo* HBP, UDP-GlcNAc and downstream CMP-Neu5Ac levels increased progressively with Gln concentrations in HeLa cells. UDP-GlcNAc levels are 2.5-fold elevated at 8 mM Gln, compared to 5.5-fold in 60 mM GlcNAc supplementation. Glc starvation in HeLa cells reduced UDP-GlcNAc by 3-fold but normalized at 6.25 mM Glc and did not increase further with Glc supply (Figure 3B).

**HBP-Dependent Effects on Metabolism.** The HBP shares intermediates with glycolysis, ammonia metabolism, and TCA cycle. UDP-GlcNAc concentrations may feed back through protein glycosylation to regulate other metabolic pathways in HeLa cells.<sup>12</sup> Our library of targeted metabolites included intermediates in these pathways, allowing us to explore interactions and dependencies on the HBP. To provide an overview of metabolite levels under the different culture conditions, the data were visualized as heat maps (Figure 4).

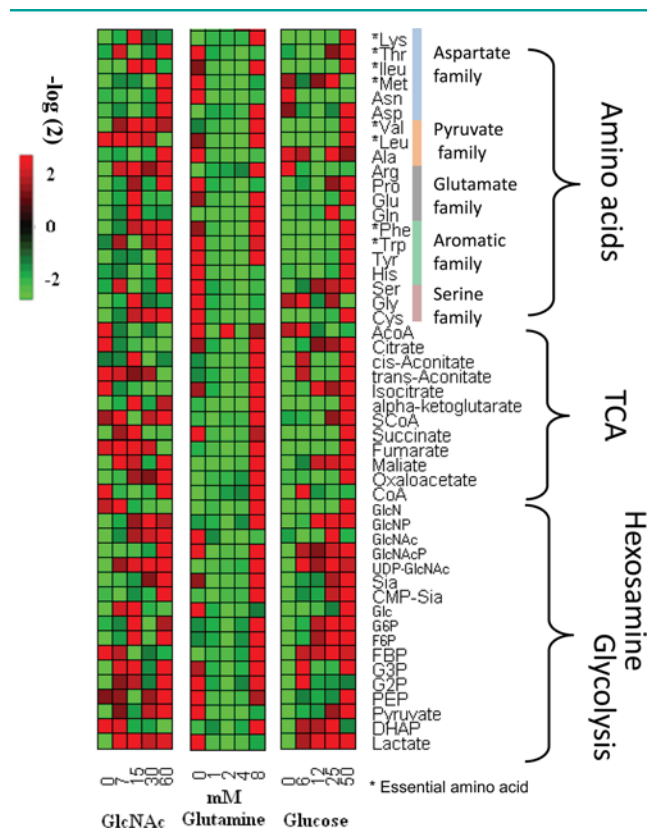


**Figure 4.** Clustered heat map of metabolite changes in HeLa cells. Metabolic profile of amino acids, TCA cycle, HBP, and glycolysis, as a function of GlcNAc (A), Gln (B), and Glc (C) titration as indicated beneath each column. The amino acids were subgrouped on the basis of their connection to the TCA and glycolysis pathway. Rows represent specific intracellular metabolites, and plotted metabolite levels are the  $\log_2$ -transformed ratio of the measured sample signal to the geometric mean signal of the metabolite across the experiment.

Changes with increasing Gln supplementation were biphasic, while Glc supplementation showed progressive increases for most metabolites, consistent with the PC analysis (Figure 2). Cellular Gln levels were maintained in conditions of Gln or Glc starvation, suggesting robust regulation of *de novo* Gln synthesis from alternate substrates (Figure 3B). However, as expected,

cell proliferation was reduced in the absence of Gln or Glc (Figure 3C). Extracellular Gln is taken up by the SLC1A5 transporter in HeLa cells, while the bidirectional transporter SLC7A5/SLC3A2, simultaneously directs efflux of Gln and uptake of essential amino acids into the cells.<sup>34</sup> Therefore the intracellular levels of Gln are coupled with the demand for essential amino acids (EAA). A more complex metabolic profile was observed with GlcNAc supplementation. Glutamine (Gln), glutamate (Glu), and the essential amino acids leucine (Leu), isoleucine (Ileu), and valine (Val) also showed biphasic response with highest levels at  $\sim 15$  mM GlcNAc and are discussed further below.

With titration of Gln, many intracellular metabolites display a biphasic response with minima at 2 mM Gln, which is the reference culture condition (Figure 4). For example, GlcP and FruP are elevated in Gln-depleted medium, and levels decline as Gln supply increases from 0 to 2 mM (Figure 3B). As Gln availability increases from 2 to 8 mM, GlcP and FruP levels increased, presumably due to the contribution of glutamine to oxidative respiration, which reduces the demand on glycolysis. Glutamate and  $\alpha$ -ketoglutarate also increased with glutamine supplementation from 4 to 8 mM, indicating an anaplerotic contribution to TCA cycle intermediates (Figure 5).

Since UDP-GlcNAc levels are sensitive to the external supplies of Glc, Gln, and GlcNAc, the subset of features common to the titrations of the metabolites may reveal pathways regulated by UDP-GlcNAc. HeLa cell metabolites were analyzed by one-way ANOVA, and the significantly changed metabolites ( $P < 0.05$ ) that overlapped were identified (Supplementary Figure S1, Table S3). The number of covarying features in pairwise manner were GlcNAc to Gln ( $n = 35$ ), GlcNAc to Glc ( $n = 28$ ), and Gln versus Glc ( $n = 7$ ). The 3-way overlap was analyzed for pathway enrichment features by Metaboanalyst,<sup>12</sup> which pointed to glutathione metabolism, implicating the TCA cycle and redox potential.

**Regulation of Redox Potential by the HBP in HeLa Cells.** A direct examination of TCA cycle metabolites revealed that oxaloacetate increased with both GlcNAc and Gln, whereas citrate levels decreased progressively with GlcNAc and displayed a biphasic response to Gln (Figure 5). The GlcNAc-mediated decrease in citrate was not accompanied by pyruvate, p-glycerate, or lactate depletion. These upstream intermediates were increased  $\sim 2$ -fold with GlcNAc titration (Supplementary Figure S2A–D). This suggests that pyruvate dehydrogenase complex (PDC) activity may be reduced, a key enzyme that converts pyruvate, CoA, and  $\text{NAD}^+$  to acetyl-CoA and NADH. PDC activity is inhibited by pyruvate dehydrogenase kinase (PDK1), and an elevated NADH/ $\text{NAD}^+$  ratio should activate PDK1. GlcNAc titration from 0 to 15 mM increased the NADH/ $\text{NAD}^+$  ratio, while 30 to 60 mM normalized the ratio (Figure 6A, Supplementary Figure S3). The decline in citrate might be due to increased TCA cycle activity, initially driving up the NADH/ $\text{NAD}^+$  ratio, followed by NADH-dependent activation of PDK1 at 30–60 mM GlcNAc, thereby inhibiting PDC and normalizing the NADH/ $\text{NAD}^+$  ratio (Figure 6A,B). The biphasic effects of glutamine titration on TCA intermediates are consistent with its conversion to  $\alpha$ -ketoglutarate and anaplerotic support for the NADH/ $\text{NAD}^+$  ratio, which shows the same dynamics.

The biphasic responses to Gln titration suggest a shift from Glc and to Gln metabolism. Similarly, the biphasic response to GlcNAc titrations may also be a similar shift from Glc to Gln and other amine acid as suggested by the heat map in Figure 4.

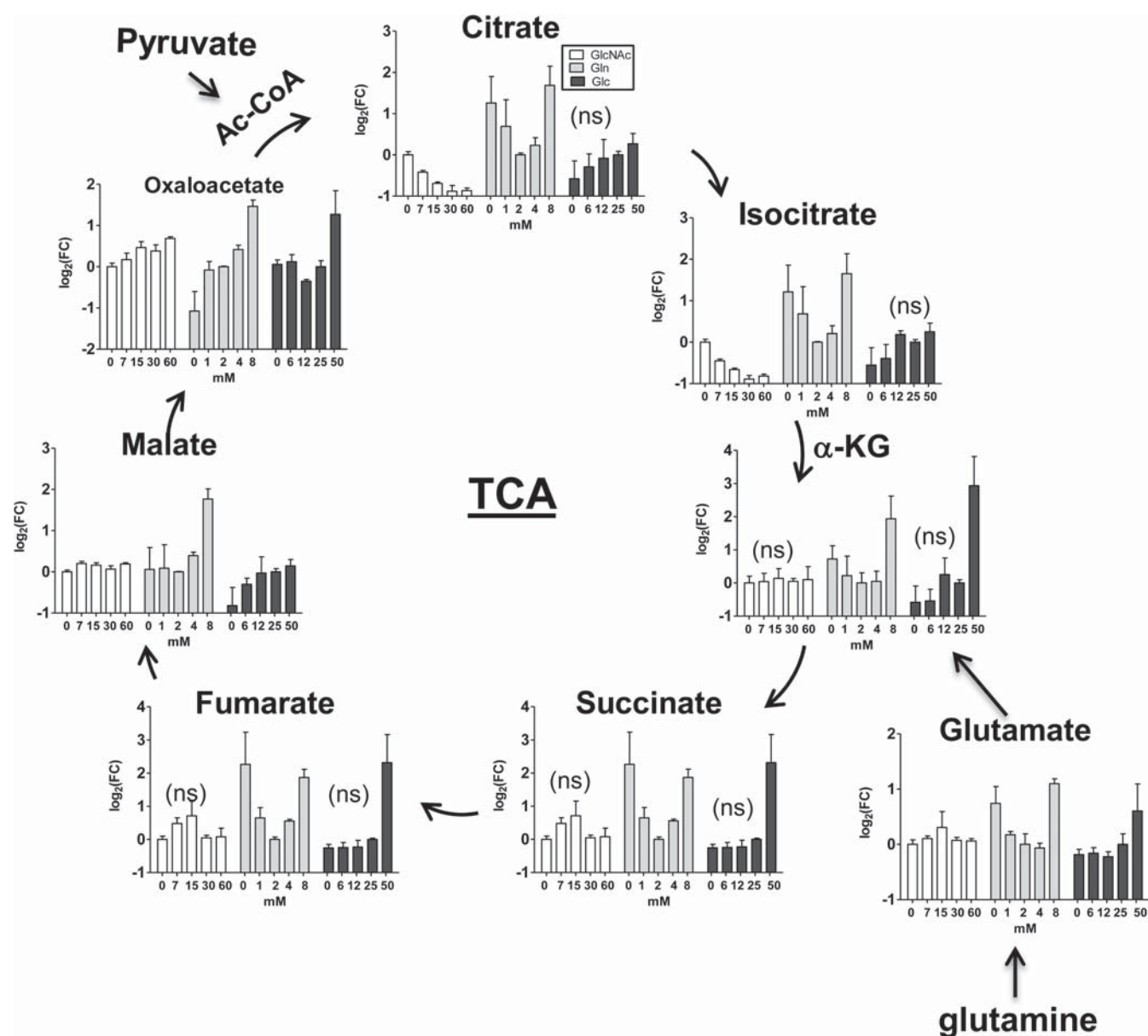


**Figure 5.** TCA cycle metabolites with GlcNAc, Gln and Glc titration in HeLa cells. Significant changes associated with the titrations were assessed by one-way ANOVA ( $P < 0.05$ ) or otherwise assigned as (ns) on the figure. The data were normalized to normal samples 1, 3, and 4 in the GlcNAc, Gln, and Glc titrations, respectively.

Gln can also support a reverse TCA-cycle reaction in cancer cells, where mitochondrial isocitrate dehydrogenase (IDH) mediates NADPH-dependent reductive carboxylation of  $\alpha$ -ketoglutarate leading to aconitase and citrate efflux.<sup>35</sup> Thus in the GlcNAc titrations, increasing Gln metabolism may follow after enhanced glycolysis and stimulate the TCA reversal reactions, thereby reducing NADPH and NADH redox potential at higher GlcNAc concentrations. As a third possibility, NADPH and NADH may be suppressed by uncoupling of oxidative phosphorylation and increased production of reactive oxygen species (ROS). ROS is largely the toxic byproducts of the electron transport chain, and glutathione (GSH) buffers against toxicity.<sup>36</sup> GSH is converted to oxidized-glutathione (GSSG) by ROS, and the reverse reaction requires NADPH to restore GSH.

Redox potential is exchanged between NADH/NAD<sup>+</sup> and NADPH/NADP<sup>+</sup> via the citrate-malate-pyruvate shuttle

operating between mitochondria and cytosol (Figure 6D). Indeed, the NADH/NAD<sup>+</sup> and NADPH/NADP<sup>+</sup> ratios in HeLa cells displayed a similar biphasic response to GlcNAc (Figure 6C). Both ROS levels and the GSH/GSSG ratio responded to GlcNAc as an inverted biphasic response (a mirror image of NADPH/NADP<sup>+</sup>). Individually, GSSG was increased, and GSH displayed reciprocal biphasic responses with optima at 15 mM GlcNAc (Supplementary Figure S3A,C). Cysteine and thiamin pyrophosphate displayed a similar inverted biphasic responses to GlcNAc, suggesting flux of these metabolite into GSH biosynthesis is also increased at 15 mM GlcNAc (Supplementary Figure S3E,F).

GlcNAc supplementation has previously been shown to increase Gln uptake in Glc-starved lymphoma cells.<sup>23</sup> Thus 15 mM GlcNAc may up-regulate Glc and Gln metabolism, thereby increasing NADH and NADPH, which suppresses ROS (Figure 6D). Interestingly, 15 mM GlcNAc corresponds to ~80% of

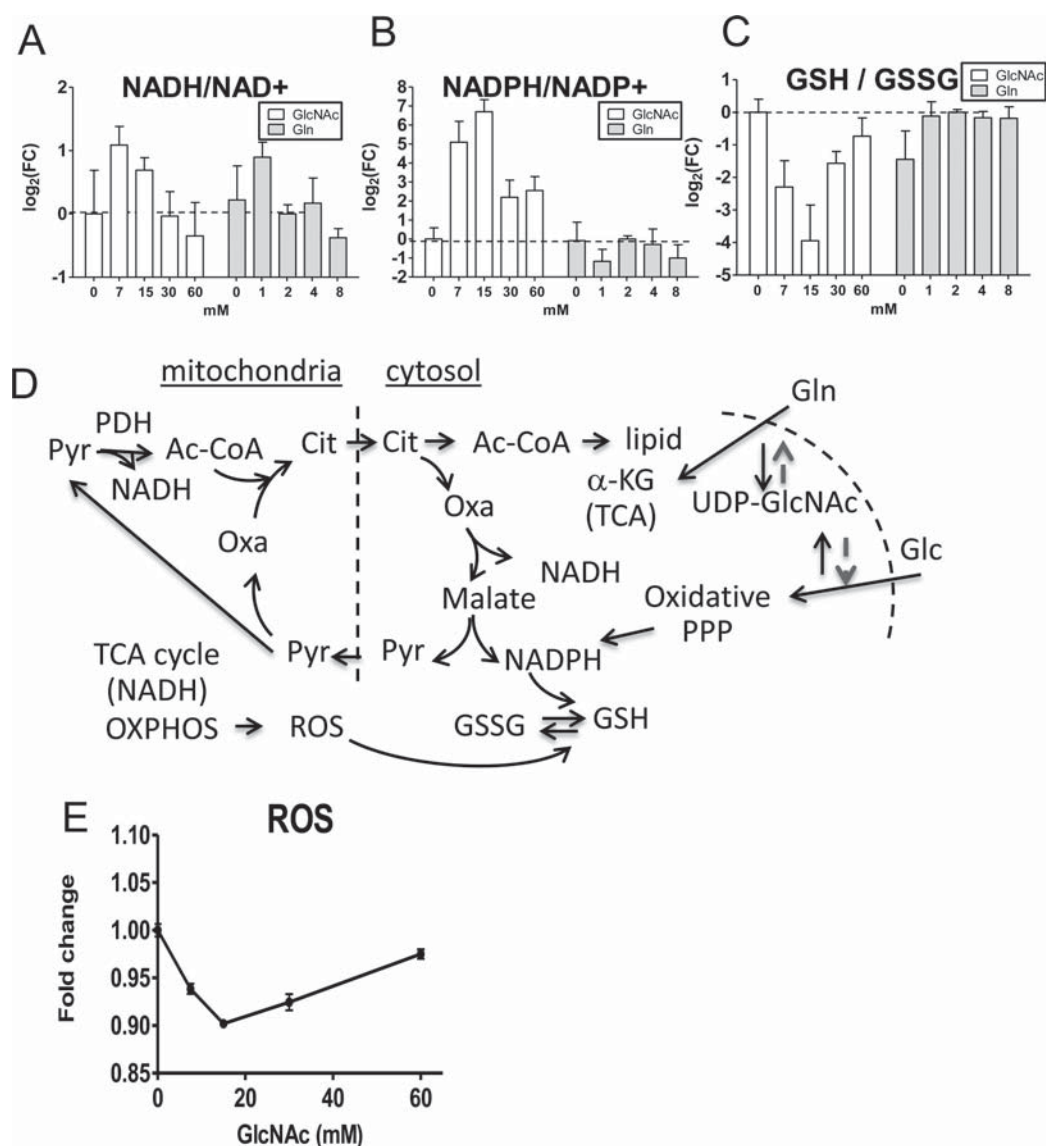


**Figure 6.** Effects of GlcNAc and Gln on redox potential in HeLa cells. (A) NADH/NAD<sup>+</sup> ratio, (B) NADPH/NADP<sup>+</sup> ratio, (C) GSH/GSSG ratio. (D) Pathways linking the observed effects of hexosamine (GlcNAc titration) on HeLa cell metabolism. The red arrow indicates unknown mechanism of UDP-GlcNAc and downstream glycoproteins on signaling and nutrient uptake.

maximal UDP-GlcNAc, with the remaining 20% occurs at 30–60 mM GlcNAc where normalization of the redox ratios is observed (Figure 3B). The Golgi *N*-glycan branching enzymes (Mgat1,2,4,5) display a 400-fold range of  $K_m$  values for UDP-GlcNAc, which plays a critical role in glycoprotein receptor and transporter levels at the cell surface.<sup>14</sup> For example, surface levels of EGF and TGF- $\beta$  receptors are optimal at different UDP-GlcNAc concentrations, and their relative levels impact growth signaling and gene expression in epithelial cell lines. Growth factor signaling to Rb-E2F1 has been shown to up-regulate PDK1 gene expression, consistent with the suppression of PDC activity and induction of the Warburg effect.<sup>37</sup> At higher concentrations of UDP-GlcNAc, TGF- $\beta$  signaling increases and may stimulate fatty acid synthesis and storage.<sup>38</sup>

**Metabolic Profile of PC-3 Prostate Tumor Cells.** To extend our analysis to other cancer cell lines, PC-3 human prostate cancer cells were prepared with the same protocol used for HeLa cells. Titration of Gln and Glc revealed that PC-3 cells were more dependent on extracellular glutamine than HeLa cells, and conversely, HeLa cells were predominantly glycolytic

as suggested by a more severe depletion of GlcP and FruP in the absence of Glc. In both cell lines, UDP-GlcNAc levels declined with Glc starvation but not glutamine depletion, whereas an excess abundance of glutamine but not Glc increased UDP-GlcNAc levels 2–3-fold. In GlcNAc supplemented PC-3 cells, larger increases in GlcNAcP, UDP-GlcNAc, and CMP-Neu5Ac were observed, and unlike HeLa cells, GlcP also increased (Supplementary Figure S5A). Mammalian tumor cell lines display very low GlcNAcP deacetylase activity based on metabolic flux analysis,<sup>23</sup> and therefore conversion to GlcNP is unlikely to account for the observed increases in GlcP and FruP. Indeed, GlcNAc supplementation caused a 400-fold increase in GlcNAcP and only a 3-fold increase in GlcNP. This small increase in GlcNP can be accounted for by the effect of increased glutamine on *de novo* HBP. In this regard, GlcNP levels are comparable for PC-3 cells in 15 mM GlcNAc or 4 mM glutamine. Unlike in HeLa cells, GlcNAc treatment increased metabolite levels widely in glycolysis, TCA cycle, amino acids, and PPP. The effect of 15 mM GlcNAc on PC-3 was comparable to increasing the availability of extracellular

Gln from 2 to 4 mM. This suggests Glc sufficiency and glutamine excess regulate *de novo* HBP, and UDP-GlcNAc supply to protein glycosylation drives positive feedback to metabolism in PC-3 tumor cells (Supplementary Figure S5B–E). The Glc transporters have only a single *N*-glycan site and are dependent on Golgi *N*-glycan branching (UDP-GlcNAc utilizing enzymes), as reported for surface residency of GLUT2 in  $\beta$ -cells,<sup>16</sup> GLUT1 in tumor cells,<sup>39</sup> and insulin- and HBP-stimulated increase in surface expression of GLUT4.<sup>14,40</sup> The cell surface levels of amino acid and other solute transporters are also dependent on UDP-GlcNAc.<sup>23,41</sup>

In conclusion, we describe a method of nutrient titration and targeted LC–MS/MS to profile tumor cell metabolism and nutrient dependencies. The method readily distinguished HeLa and PC-3 tumor cells. Our data also suggest that HBP is a potential target in cancer metabolism that might be exploited for novel cancer therapies.<sup>36</sup> For example, inhibition of the HBP in tumors with PC-3-like metabolism may suppress metabolism and down-regulate cell growth. Alternatively, GlcNAc supplementation in tumor cells with a HeLa-like metabolic profile may sensitize them to compounds that create a redox imbalance, such as inhibition of lactate dehydrogenase, oxidative respiration, or uncoupling agents. For instance, inhibition of PDK with dichloroacetate (DCA) in hypoxic cancer cells can increase production of ROS and promote tumor cell death.<sup>36</sup> Inhibitors of NADPH production by the PPP or disruption of GSH synthesis may also lead to tumor cell death. Our results provide a method of identifying tumor subtypes by metabolic profiling and a basis for screening to identify chemical modifiers that may have synthetic-lethal and tumor-selective effects on tumor cells.

## METHODS

Metabolite standards and reagents were obtained from Sigma Chemicals (St. Louis, MO) in minimal purity (98%). Isotope-labeled metabolites were purchased from Cambridge Isotope, Inc. (Woburn, MA). All organic solvents and water used in sample and LC–MS mobile phase preparation were HPLC grade and obtained from Fisher Scientific (Fair Lawn, NJ).

**Standard Solutions and MS Tuning.** Stock solutions were prepared for each metabolite standard at a concentration of 100  $\mu$ M in 40/60 methanol/water (v/v), 0.1% NaOH. A final concentration (10  $\mu$ M) of each metabolite was obtained for mass spectrometric tuning. A standard mixture of all metabolites was prepared at 75, 250, and 1500 nM as a sensitivity and specificity quality control. Ten additional serially diluted samples were prepared ranging from 1 nM to 2  $\mu$ M for linearity assessments. A mixture of all standard metabolites was used daily to check the LC–MS/MS system for optimal ionization polarity, declustering potential (DP), precursor ion (Q1), product ion (Q1), and collision energy (CE). Ion source potential (ISP) was 4500 V for positive and negative modes. Nebulizer gas (GS1) and bath gas (GS2) were 10 psi, curtain gas (CUR) was 15 psi, and collision gas (CAD) was 4 psi. Source temperature (TEM) was set to zero, and interface heater was ON. The mass spectrometry is maintained calibrated using a special kit designed by the manufacturer (ABSciex, Canada)

**HeLa and PC-3 Cell Cultures and Metabolite Extraction.** HeLa cells are a human cervical cancer cell line, typically cultured in DMEM and 10% FBS. HeLa cells were cultured in an incubator at 37 °C for 24 h in 6-well plates (6-WP) with five different concentrations of each nutrient/supplement: GlcNAc at 0, 7.5, 15, 30, and 60 mM; Gln at 0, 1, 2, 4, and 8 mM; and Glc at 0, 6.25, 12.5, 25, and 50 mM. These modifications were made to the reference DMEM 10% FBS medium, containing 25 mM Glc, 2 mM Gln, and 0 mM GlcNAc. After 24 h of incubation with these nutrient/supplement media, the media was aspirated, and cells were washed on the plates with warm phosphate buffer saline (PBS) two times. The metabolites were

extracted by addition of 1 mL of an ice-cold solution of 40% acetonitrile, 40% methanol, and 20% water containing internal standards (500  $\mu$ g/mL and 300  $\mu$ g/mL of D<sub>7</sub>-glucose and <sup>13</sup>C,<sup>15</sup>N-tyrosine, respectively). After quenching the cells were scraped and transferred to 1.5 mL tubes and shaken for 1 h at 4 °C and 1000 rpm in a Thermomixer (Eppendorf, Germany). The samples were spun down at 14000 rpm for 10 min at 4 °C (Eppendorf, Germany), and then the supernatant was transferred to fresh tubes to be evaporated to dryness in a CentreVap concentrator at 40 °C (Labconco, MO). The dry extract samples were stored at –80 °C for LC–MS analysis. Cell number for each condition was determined by trypsinization of parallel replicate wells. The same reference medium and procedure was used for the PC-3 prostate cancer cell line using the critical titration points: GlcNAc at 0, 15, and 30 mM; Gln at 0, 2, and 4 mM; and Glc at 0, 12.5, and 25 mM. Variation in the procedure was examined with technical replicates done on 3 cell lines and extracted on successive days (Supplementary Figure S4).

**Sample Reconstitution and LC–MS/MS Analysis.** The dry metabolite extracts were reconstituted in 200  $\mu$ L of water. The mixture of metabolites was injected twice through the HPLC (Dionex Corporation, CA) in gradient reversed phase column Inertsil ODS-3, 4.6 mm internal diameter, 150 mm length, and 3  $\mu$ m particle size for positive and negative mode analysis. In positive mode analysis, the mobile phase gradient ramps from 5% to 90% of acetonitrile in 16 min, and after 1 min at 90%, the composition returns to 5% acetonitrile in 0.1% acetic acid in 2 min. In negative mode, the acetonitrile composition ramps from 5% to 90% in 10 min, and after 1 min at 90%, the gradient ramps back to 5% acetonitrile in buffer A (0.1% tributylamine, 0.03% acetic acid, 15% methanol). The total runtime in both modes was 20 min, the samples were stored at 4 °C, and the injection volume was 10  $\mu$ L. An automated washing procedure was developed before and after each sample to avoid any sample carryover.

The eluted metabolites were analyzed at the optimum polarity in MRM mode on electrospray ionization (ESI) triple-quadrupole mass spectrometer (ABSciex4000Qtrap, Toronto, ON, Canada). The mass spectrometric data acquisition time for each run was 20 min, and the dwell time for each MRM channel was 10 ms. Common mass spectrometric parameters were the same as tuning conditions described above, with the exception that GS1 and GS2 were 50 psi; CUR was 20 psi, and CAD was 3 and 7 for positive and negative modes, respectively, and source temperature (TEM) was 400 °C.

**Data Acquisition, Processing, and Visualization.** An injection program was developed on HPLC using Chromeleon Client version 6.8 (Dionex Corporation, CA) to introduce samples into the mass spectrometer for detection using Analyst version 1.5.2 (ABSciex, Toronto, ON, Canada). The raw data was imported to MultiQuant version 2.0.0 (ABSciex, Toronto, ON, Canada), and the extracted ion chromatogram (XIC) peaks of metabolites were integrated. Area under the peak is used as quantitative measurement for assay performance such as linearity, sensitivity, and reproducibility.

The result table contains the area, area ratio (area of analyte/area of internal standard), retention time, and concentration and is then exported from MultiQuant as text files to MarkerView version 1.2.11 (ABSciex, Toronto, ON, Canada) for normalization with cell number and protein content and then subsequent PCA cluster analysis. Further analysis was done with MetaboAnalyst (<http://www.metaboanalyst.ca/MetaboAnalyst/>), an online software program for statistical analysis, normalization, graphing, sample clustering, heat maps, and pathway analysis based on KEGG databases (<http://www.genome.jp/kegg/pathway.html>).<sup>24,32</sup>

**Measurement of Reactive Oxygen Species.** To detect reactive oxygen species (ROS), reagent 2',7'-dichlorodihydrofluorescein diacetate (DCF) from Invitrogen was used according to manufacturer's specifications. Briefly, HeLa cells were seeded in a 96-well plate in standard high-glucose DMEM media with 10% FBS and treated with various concentrations of GlcNAc for 24 h. The growth media was then removed from the cells and replaced with prewarmed PBS containing DCF probe at 10  $\mu$ M. The cells were then incubated for 1 h at 37 °C in 5% CO<sub>2</sub>. The PBS loading buffer containing DCF probe was then removed and replaced with regular high-glucose DMEM

media with 10% FBS for an additional 30 min, after which the ROS was measured on Flex Station 3 benchtop multimode microplate reader (Molecular Devices, Sunnyvale, CA) with excitation and emission of 490 nm and 530 nm, respectively.

## ■ ASSOCIATED CONTENT

### ■ Supporting Information

A list of targeted metabolites measured by mass spectrometry, their instrumental parameters, and database accession numbers; a list of HeLa cell metabolites sensitive to the extracellular GlcNAc, Gln, and Glc; and supplemental data for HeLa and PC3 tumor cells. This material is available free of charge via the Internet at <http://pubs.acs.org>.

## ■ AUTHOR INFORMATION

### Corresponding Author

\*E-mail: [dennis@lunenfeld.ca](mailto:dennis@lunenfeld.ca).

### Notes

The authors declare no competing financial interest.

## ■ ACKNOWLEDGMENTS

The authors thank Kevin Yau and Amy Woroch for valuable technical assistance. Research was supported by grants from Canadian Cancer Society (2010-7000444), MRI-ORF GL2 and CIHR (MOP-62975) to J.W.D. A.A.R. was supported by MITACS-Accelerate, and M.R. was supported by the Frank Fletcher Memorial Fund, Joseph Bazylewicz Scholarship, Mary Gertrude l'Anson Scholarship, and Paul Starita Graduate Student Fellowship.

## ■ REFERENCES

- (1) Levine, A. J., and Puzio-Kuter, A. M. (2010) The control of the metabolic switch in cancers by oncogenes and tumor suppressor genes. *Science* 330, 1340–1344.
- (2) DeBerardinis, R. J., Lum, J. J., Hatzivassiliou, G., and Thompson, C. B. (2008) The biology of cancer: metabolic reprogramming fuels cell growth and proliferation. *Cell Metab.* 7, 11–20.
- (3) Vander Heiden, M. G., Cantley, L. C., and Thompson, C. B. (2009) Understanding the Warburg effect: the metabolic requirements of cell proliferation. *Science* 324, 1029–1033.
- (4) Vander Heiden, M. G., Locasale, J. W., Swanson, K. D., Sharfi, H., Heffron, G. J., Amador-Noguez, D., Christofk, H. R., Wagner, G., Rabinowitz, J. D., Asara, J. M., and Cantley, L. C. (2010) Evidence for an alternative glycolytic pathway in rapidly proliferating cells. *Science* 329, 1492–1499.
- (5) Ye, J., Mancuso, A., Tong, X., Ward, P. S., Fan, J., Rabinowitz, J. D., and Thompson, C. B. (2012) Pyruvate kinase M2 promotes de novo serine synthesis to sustain mTORC1 activity and cell proliferation. *Proc. Natl. Acad. Sci. U.S.A.* 109, 6904–6909.
- (6) Li, T., Kon, N., Jiang, L., Tan, M., Ludwig, T., Zhao, Y., Baer, R., and Gu, W. (2012) Tumor suppression in the absence of p53-mediated cell-cycle arrest, apoptosis, and senescence. *Cell* 149, 1269–1283.
- (7) DeBerardinis, R. J., Mancuso, A., Daikhin, E., Nissim, I., Yudkoff, M., Wehrli, S., and Thompson, C. B. (2007) Beyond aerobic glycolysis: transformed cells can engage in glutamine metabolism that exceeds the requirement for protein and nucleotide synthesis. *Proc. Natl. Acad. Sci. U.S.A.* 104, 19345–19350.
- (8) Kalaany, N. Y., and Sabatini, D. M. (2009) Tumours with PI3K activation are resistant to dietary restriction. *Nature* 458, 725–731.
- (9) Yun, J., Rago, C., Cheong, I., Pagliarini, R., Angenendt, P., Rajagopalan, H., Schmidt, K., Willson, J. K., Markowitz, S., Zhou, S., Diaz, L. A., Jr., Velculescu, V. E., Lengauer, C., Kinzler, K. W., Vogelstein, B., and Papadopoulos, N. (2009) Glucose deprivation contributes to the development of KRAS pathway mutations in tumor cells. *Science* 325, 1555–1559.
- (10) Ying, H., Kimmelman, A. C., Lyssiotis, C. A., Hua, S., Chu, G. C., Fletcher-Sananikone, E., Locasale, J. W., Son, J., Zhang, H., Coloff, J. L., Yan, H., Wang, W., Chen, S., Viale, A., Zheng, H., Paik, J. H., Lim, C., Guimaraes, A. R., Martin, E. S., Chang, J., Hezel, A. F., Perry, S. R., Hu, J., Gan, B., Xiao, Y., Asara, J. M., Weissleder, R., Wang, Y. A., Chin, L., Cantley, L. C., and DePinho, R. A. (2012) Oncogenic Kras maintains pancreatic tumors through regulation of anabolic glucose metabolism. *Cell* 149, 656–670.
- (11) Helenius, A., and Aebi, M. (2004) Roles of N-linked glycans in the endoplasmic reticulum. *Annu. Rev. Biochem.* 73, 1019–1049.
- (12) Dennis, J. W., Nabi, I. R., and Demetriou, M. (2009) Metabolism, cell surface organization, and disease. *Cell* 139, 1229–1241.
- (13) Hart, G. W., Housley, M. P., and Slawson, C. (2007) Cycling of O-linked beta-N-acetylglucosamine on nucleocytoplasmic proteins. *Nature* 446, 1017–1022.
- (14) Lau, K., Partridge, E. A., Grigorian, A., Silvescu, C. I., Reinhold, V. N., Demetriou, M., and Dennis, J. W. (2007) Complex N-glycan number and degree of branching cooperate to regulate cell proliferation and differentiation. *Cell* 129, 123–124.
- (15) Kreppel, L. K., and Hart, G. W. (1999) Regulation of a cytosolic and nuclear O-GlcNAc transferase. Role of the tetratricopeptide repeats. *J. Biol. Chem.* 274, 32015–32022.
- (16) Ohtsubo, K., Ohtsubo, K., Takamatsu, S., Minowa, M. T., Yoshida, A., Takeuchi, M., and Marth, J. D. (2005) Dietary and genetic control of glucose transporter 2 glycosylation promotes insulin secretion in suppressing diabetes. *Cell* 123, 1307–1321.
- (17) Boscher, C., Zheng, Y. Z., Lakshminarayan, R., Johannes, L., Dennis, J. W., Foster, L. J., and Nabi, I. R. (2012) Galectin-3 regulates mobility of N-cadherin and GM1 ganglioside at cell-cell junctions of mammary carcinoma cells. *J. Biol. Chem.* 287, 32940–32952.
- (18) Lajoie, P., Partridge, E. A., Guay, G., Goetz, J. G., Pawling, J., Lagana, A., Joshi, B., Dennis, J. W., and Nabi, I. R. (2007) Plasma membrane domain organization regulates EGFR signaling in tumor cells. *J. Cell. Biol.* 179, 341–356.
- (19) Broschat, K. O., Gorka, C., Page, J. D., Martin-Berger, C. L., Davies, M. S., Huang, H. C., Gulve, E. A., Salsgiver, W. J., and Kastan, T. P. (2002) Kinetic characterization of human glutamine-fructose-6-phosphate amidotransferase I: potent feedback inhibition by glucosamine 6-phosphate. *J. Biol. Chem.* 277, 14764–14770.
- (20) Oikawa, S., Sato, H., and Akamatsu, N. (1986) Glucosamine 6-phosphate acetylase in rat ascites hepatomas. *Int. J. Biochem.* 18, 929–933.
- (21) Alvarez, F. J., and Konopka, J. B. (2007) Identification of an N-acetylglucosamine transporter that mediates hyphal induction in *Candida albicans*. *Mol. Biol. Cell* 18, 965–975.
- (22) Breidenbach, M. A., Gallagher, J. E., King, D. S., Smart, B. P., Wu, P., and Bertozzi, C. R. (2010) Targeted metabolic labeling of yeast N-glycans with unnatural sugars. *Proc. Natl. Acad. Sci. U.S.A.* 107, 3988–3993.
- (23) Wellen, K. E., Lu, C., Mancuso, A., Lemons, J. M., Ryczko, M., Dennis, J. W., Rabinowitz, J. D., Collier, H. A., and Thompson, C. B. (2010) The hexosamine biosynthetic pathway couples growth factor-induced glutamine uptake to glucose metabolism. *Genes Dev.* 24, 2784–2799.
- (24) Xia, J., Mandal, R., Sinelnikov, I. V., Broadhurst, D., and Wishart, D. S. (2012) MetaboAnalyst 2.0: a comprehensive server for metabolomic data analysis. *Nucleic Acids Res.* 40, W127–133.
- (25) Xia, J., and Wishart, D. S. (2011) Web-based inference of biological patterns, functions and pathways from metabolomic data using MetaboAnalyst. *Nat. Protoc.* 6, 743–760.
- (26) Tautenhahn, R., Cho, K., Uritboonthai, W., Zhu, Z., Patti, G. J., and Siuzdak, G. (2012) An accelerated workflow for untargeted metabolomics using the METLIN database. *Nat. Biotechnol.* 30, 826–828.
- (27) Wishart, D. S., Knox, C., Guo, A. C., Eisner, R., Young, N., Gautam, B., Hau, D. D., Psychogios, N., Dong, E., Bouatra, S., Mandal, R., Sinelnikov, I., Xia, J., Jia, L., Cruz, J. A., Lim, E., Sobsey, C. A., Shrivastava, S., Huang, P., Liu, P., Fang, L., Peng, J., Fradette, R.,

Cheng, D., Tzur, D., Clements, M., Lewis, A., De Souza, A., Zuniga, A., Dawe, M., Xiong, Y., Clive, D., Greiner, R., Nazyrova, A., Shaykhtudinov, R., Li, L., Vogel, H. J., and Forsythe, I. (2009) HMDB: a knowledgebase for the human metabolome. *Nucleic Acids Res.* 37, D603–610.

(28) Yuan, M., Breitkopf, S. B., Yang, X., and Asara, J. M. (2012) A positive/negative ion-switching, targeted mass spectrometry-based metabolomics platform for bodily fluids, cells, and fresh and fixed tissue. *Nat. Protoc.* 7, 872–881.

(29) Reitzer, L. J., Wice, B. M., and Kennell, D. (1979) Evidence that glutamine, not sugar, is the major energy source for cultured HeLa cells. *J. Biol. Chem.* 254, 2669–2676.

(30) Piva, T. J., and McEvoy-Bowe, E. (1998) Oxidation of glutamine in HeLa cells: role and control of truncated TCA cycles in tumour mitochondria. *J. Cell. Biochem.* 68, 213–225.

(31) Sasai, K., Ikeda, Y., Fujii, T., Tsuda, T., and Taniguchi, N. (2002) UDP-GlcNAc concentration is an important factor in the biosynthesis of beta1,6-branched oligosaccharides: regulation based on the kinetic properties of N-acetylglucosaminyltransferase V. *Glycobiology* 12, 119–127.

(32) Xia, J., Psychogios, N., Young, N., and Wishart, D. S. (2009) MetaboAnalyst: a web server for metabolomic data analysis and interpretation. *Nucleic Acids Res.* 37, W652–660.

(33) Galeano, B., Klootwijk, R., Manoli, I., Sun, M., Ciccone, C., Darvish, D., Starost, M. F., Zerfas, P. M., Hoffmann, V. J., Hoogstraten-Miller, S., Krasnewich, D. M., Gahl, W. A., and Huizing, M. (2007) Mutation in the key enzyme of sialic acid biosynthesis causes severe glomerular proteinuria and is rescued by N-acetylmannosamine. *J. Clin. Invest.* 117, 1585–1594.

(34) Nicklin, P., Bergman, P., Zhang, B., Triantafellow, E., Wang, H., Nyfeler, B., Yang, H., Hild, M., Kung, C., Wilson, C., Myer, V. E., MacKeigan, J. P., Porter, J. A., Wang, Y. K., Cantley, L. C., Finan, P. M., and Murphy, L. O. (2009) Bidirectional transport of amino acids regulates mTOR and autophagy. *Cell* 136, 521–534.

(35) Smolkova, K., and Jezek, P. (2012) The role of mitochondrial NADPH-dependent isocitrate dehydrogenase in cancer cells. *Int. J. Cell Biol.*, DOI: 10.1155/2012/273947.

(36) Schulze, A., and Harris, A. L. (2012) How cancer metabolism is tuned for proliferation and vulnerable to disruption. *Nature* 491, 364–373.

(37) Hsieh, M. C., Das, D., Sambandam, N., Zhang, M. Q., and Nahle, Z. (2008) Regulation of the PDK4 isozyme by the Rb-E2F1 complex. *J. Biol. Chem.* 283, 27410–27417.

(38) Yadav, H., Quijano, C., Kamaraju, A. K., Gavrilova, O., Malek, R., Chen, W., Zerfas, P., Zhigang, D., Wright, E. C., Stuelten, C., Sun, P., Lonning, S., Skarulis, M., Sumner, A. E., Finkel, T., and Rane, S. G. (2011) Protection from obesity and diabetes by blockade of TGF-beta/Smad3 signaling. *Cell. Metab.* 14, 67–79.

(39) Kitagawa, T., Tsuruhara, Y., Hayashi, M., Endo, T., and Stanbridge, E. J. (1995) A tumor-associated glycosylation change in the glucose transporter GLUT1 controlled by tumor suppressor function in human cell hybrids. *J. Cell Sci.* 108, 3735–3743.

(40) Haga, Y., Ishii, K., and Suzuki, T. (2011) N-Glycosylation is critical for the stability and intracellular trafficking of glucose transporter GLUT4. *J. Biol. Chem.* 286, 31320–31327.

(41) Zhu, J., Yan, J., and Thornhill, W. B. (2012) N-Glycosylation promotes the cell surface expression of Kv1.3 potassium channels. *FEBS J.* 279, 2632–2644.